Physica E: Low-dimensional Systems and Nanostructures 98 (2018) 148–158

Contents lists available at ScienceDirect

Physica E: Low-dimensional Systems and Nanostructures

journal homepage: www.elsevier.com/locate/physe

Improved incorporation of strain gradient elasticity in the flexoelectricity based energy harvesting from nanobeams

Yarong Zhou [a], Xu Yang [a], Dongmei Pan [b], Binglei Wang [a,c,*]

[a] School of Civil Engineering, Shandong University, Jinan, 250061, China
[b] Department of Civil and Environmental Engineering, University of Houston, Houston, TX 77204, USA
[c] Department of Mechanical Engineering, University of Houston, Houston, TX 77204, USA

ARTICLE INFO

Keywords:
Flexoelectricity
Strain gradient elasticity
Energy harvesting
Piezoelectricity

ABSTRACT

Flexoelectricity, the coupling of strain gradient and polarization, exists in all the dielectric materials and numerous models have been proposed to study this mechanism. However, the contribution of strain gradient elasticity has typically been underestimated. In this work, inspired by the one-length scale parameter model developed by Deng et al. [19], we incorporate three length-scale parameters to carefully capture the contribution of the purely mechanical strain gradients on flexoelectricity. This three-parameter model is more flexible and could be applied to investigate the flexoelectricity in a wide range of complicated deformations. Accordingly, we carry out our analysis by studying a dielectric nanobeam under different boundary conditions. We show that the strain gradient elasticity and flexoelectricity have apparent size effects and significant influence on the electro-mechanical response. In particular, the strain gradient effects could significantly reduce the energy efficiency, indicating their importance and necessity. This work may be helpful in understanding the mechanism of flexoelectricity at the nanoscale and sheds light on the flexoelectricity energy harvesting.

1. Introduction

Piezoelectricity, one of most important electromechanical coupling phenomena in dielectric materials, has received wide attention in multiple fields including energy harvesting, sensing and actuation, artificial muscles, advanced microscopes among others [1–3]. For a piezoelectric material, the induced polarization ($\boldsymbol{P}$) is related to the strain ($\boldsymbol{\varepsilon}$) through a third-order piezoelectric tensor ($\boldsymbol{d}$):

$$P_i = d_{ijk}\varepsilon_{jk} \tag{1}$$

For the dielectric structures in the sub-micron or nano-scale, flexoelectricity, an interesting electro-mechanical coupling phenomenon, has received much attention in the past recent years. Flexoelectricity [4] is a type of electro-mechanical coupling mechanism that provides a linkage between the mechanical strain gradient ($\nabla\boldsymbol{\varepsilon}$) and the polarization ($\boldsymbol{P}$), namely

$$P_i = d_{ijk}\varepsilon_{jk} + f_{ijkl}\frac{\partial \varepsilon_{jk}}{\partial x_l} \tag{2}$$

where f_{ijkl} is the fourth-order flexoelectric tensor.

In the field of piezoelectricity, much effort has been devoted to improving the piezoelectric coefficient so as to maximize the piezoelectric response. Such efforts have largely been exhausted. Flexoelectricity, however, is relatively still unexplored and has promise in enhancing polarization due to its ubiquitous existence in all dielectric materials regardless of their crystal structure because the presence of strain gradient breaks the inversion symmetry of the material [5]. Furthermore, this effect is noteworthy at the nanoscale since the strain gradient is inversely proportional to the feature scale of the structures [4]. Flexoelectricity has been observed experimentally in liquid crystals [6], polymers [7], crystalline materials [8], and biomembranes [4]. Therefore, in the past few decades, flexoelectricity has been intensively studied theoretically [9–13], or numerically [14,15] and experimentally [8,16] from both fundamental and applicable points of view. Recently, Krichen and Sharma [17] wrote a perspective on an unusual electro-mechanical coupling called flexoelectricity that has tantalizing implications in topics ranging from biophysics to the design of next-generation multifunctional nanomaterials.

Some efforts have been devoted to establishing theoretical frameworks for dielectrics with the consideration of electromechanical coupling in soft dielectrics due to their conceptual foundation and

* Corresponding author. School of Civil Engineering, Shandong University, Jinan, 250061, China.
E-mail address: bwang@sdu.edu.cn (B. Wang).

https://doi.org/10.1016/j.physe.2017.12.037
Received 25 November 2017; Received in revised form 26 December 2017; Accepted 29 December 2017
Available online 31 December 2017
1386-9477/

essential application including the instability and energy harvesting [13, 18–21]. To interpret flexoelectricity in dielectrics theoretically, Kogan [22] formulated the first phenomenological theory of flexoelectricity in 1964 and estimated the value range of flexoelectric coefficients. Sharma et al. [13] developed a theory considering first gradients of the strain and the polarization and analyzed the size-dependent mechanical and electrical behavior of piezoelectric and non-piezoelectric nanostructures theoretically and numerically. Shen and Hu [10] established a comprehensive framework for nanoscale dielectrics to study the flexoelectric response with consideration of the surface effect. Recently, Liu And Sharma [23] succeeded in establishing emergent electromechanical coupling of electrets and some exact relations - the effective properties of soft materials with embedded external charges and dipoles.

As flexoelectricity is mathematically related to strain gradients, to better understand flexoelectricity, it is best first to allude to the traditional strain gradient elasticity theory (or the non-local theory). The background of introducing the strain gradient elasticity theory is based on two facts. Firstly, size-dependent physical properties of micro/nano-scale structures are observed experimentally in metals [24,25], brittle materials [26], polymers [27] and polysilicon [28], which cannot be explained using the classical continuum theory, which has no material length scale parameters. Of course, similar to the strain gradient elasticity theory, some other theories like couple stress theory, nonlocal theory, surface energy theory are also used to capture the size effects. For the discussions and comparisons among these theories, the interested reader is referred to a related work [29] for details. Secondly, the variable in energy density for the conventional continuum theory is only the strain (first gradient of deformation). According to the Taylor series expansion mathematically, the strain gradient (second gradient of deformation) is reasonable to be included in energy density to characterize the size-dependent properties since the classical continuum theory fails. The strain gradient elasticity theory was firstly proposed by Mindlin [30] to describe the linear elastic behavior of microstructures. This theory requires 16 additional independent length-scale parameters for isotropic materials in addition to two Lame constants. Then, Mindlin and Eshel [31] further formulated it to be a simpler version, which reduces the length-scale parameters from 16 to 5 for isotropic materials. However, the application of this theory in engineering is limited as five length-scale parameters are difficult to be determined experimentally. Recently, Zhou and his co-workers [32] proved that only three length-scale parameters are independent by applying two sets of orthogonal decompositions of the strain gradient tensor. While the nonlocal theory [33], couple stress theory [34] and surface energy theory [35] have one length-scale parameter respectively.

Actually, one length-scale parameter can be experimentally determined by a simple bending or torsion test. For example, it has been demonstrated by Fleck and Hutchinson [36] that a single length-scale parameter does not have a scope to include the wide range of small-scale phenomena. Therefore, the strain gradient theory with multiple length-scale parameters is necessary to capture the size effects of mechanical and electric behavior at micro/nano-scale structures.

A recent work by Deng [5] pointed out that most of the previous works ignored the effect of strain gradient elasticity (the term $\frac{1}{2}\nabla\nabla\mathbf{u}\cdot g\nabla\nabla\mathbf{u}$ in energy density) that restricts the further increasing of strain gradients in flexoelectricity. It is well accepted that the material would become harder to deform as the decrease of the sample size due to the strain gradient elasticity. In the works of Yan and Jiang [37,38], the flexoelectric response of electroelastic and dynamic piezoelectric nanobeams are studied. The Timoshenko dielectric beam and piezoelectric nano-plate with flexoelectricity are also conducted by Zhang et al. [39]. These works, however, did not consider the effect of strain gradient elasticity theory. Deng and Sharma [19] are the first to study the energy harvesting of the nano-beam and truncated cone due to flexoelectricity with consideration of the strain gradient theory, in which the one length-scale parameter strain gradient model is used. This may lack the ability to capture the wide range of small-scale phenomena [32].

The rest of the paper is organized as follows. In Section 2, we recall the formulations of dielectric structures and followed by deriving the piezoelectric and flexoelectric nanobeam model with reformulated strain gradient elasticity theory included in Section 3. Subsequently, numerical results and discussions are then given in Section 4. Finally, some major conclusions are summarized in section 5.

2. Recalling the formulations of dielectric structure

For the electrostatic field of dielectric materials, the Gauss's law is given as

$$div\,\mathbf{D} = \rho_f \tag{3}$$

Where $\mathbf{D}$ is electric displacement vector, ρ_f is density of free charges (per unit volume). In vacuum $\rho_f = 0$, while in dielectric materials $\rho_f \neq 0$. In a polarized material, the electric polarization $\mathbf{P}$ is defined by

$$\mathbf{P} = \mathbf{D} - e_0\mathbf{E} \tag{4}$$

Where $\boldsymbol{E}$ is electric field, $e_0 = 8.85 \times 10^{-12}\,F/m$ is the permittivity of the vacuum or air.

Neglecting fringing fields, Hamilton's principle for a dielectric structure occupying the domain Ω with flexoelectricity can be written as [5].

$$\delta\int_{t_0}^{t_1}dt\int_{\Omega}\left(\frac{1}{2}\rho|\dot{\mathbf{u}}|^2 - \mathbf{U} + \frac{e_0}{2}|\mathbf{E}|^2 + \mathbf{E}\cdot\mathbf{P}\right)dV + \int_{t_0}^{t_1}dt\int_{\Omega}(\mathbf{q}\cdot\delta\mathbf{u} + \mathbf{E}^0\cdot\delta\mathbf{P})dV + \int_{t_0}^{t_1}dt\int_{\partial\Omega}\mathbf{t}_0\cdot\delta\mathbf{u}da = 0 \tag{5}$$

where $\mathbf{u}$ is displacement vector, $\mathbf{E}$ is electric field, $\mathbf{P}$ is polarization density, $\mathbf{U}$ is the internal energy density, $\mathbf{q}$ and $\mathbf{E}^0$ are the external body force and external electric field, $\mathbf{t}_0$ is surface traction.

In dealing with the problem of piezoelectric nanobeam with the consideration of the flexoelectricity, our mathematical modeling is based on the extended liner theory of piezoelectricity, in which the strain gradient elasticity is incorporated. The general expression for the internal energy density $\boldsymbol{U}$ can be written as

$$U = \frac{1}{2}\boldsymbol{\varepsilon}\cdot c\boldsymbol{\varepsilon} + \frac{1}{2}\mathbf{P}\cdot a\mathbf{P} + \frac{1}{2}\nabla\nabla\mathbf{u}\cdot g\nabla\nabla\mathbf{u} + \boldsymbol{\varepsilon}\cdot d\mathbf{P} + \mathbf{P}\cdot f\nabla\nabla\mathbf{u} \tag{6}$$

where ε_{ij} and P_i are the components for the strain tensor and polarization vector, while u_i are the components for the displacement vector. c_{ijkl}, a_{kl} and d_{ijk} are the components of the fourth-order elastic coefficient, second-order reciprocal dielectric susceptibility and three-order piezoelectric coefficient tensors respectively. These material constant tensors are exactly the same as those in the liner piezoelectricity theory. f_{ijkl} are the components in the polarization and strain gradient coupling tensor, i.e., the flexo-coupling coefficient. The components g_{ijklmn} represents the purely nonlocal elastic effects and relates to the strain gradient elasticity theory.

Thus, the independent variables in the internal energy density $\boldsymbol{U}$ are strain, strain gradient and polarization. The corresponding stress, higher order stress and electric field, which are work-conjugated to strain, strain gradient and polarization, are expressed as

$$\sigma_{ij} = \frac{\partial U}{\partial\varepsilon_{ij}} = c_{ijkl}\varepsilon_{kl} + d_{ijk}P_k \tag{7}$$

$$\sigma_{ijm} = \frac{\partial U}{\partial u_{i,jm}} = f_{ijmk}P_k + g_{ijmknl}u_{k,nl} \tag{8}$$

$$E_i = \frac{\partial U}{\partial P_i} = a_{ij}P_j + d_{jki}\varepsilon_{jk} + f_{ijkl}u_{j,kl} \tag{9}$$

where a comma followed by a subscript denotes differentiation with respect to the subscript. σ_{ij} is the traditional stress tensor, and σ_{ijm} is defined as the higher order stress or the moment stress, which is induced by the flexoelectric and strain gradient effects while does not exist in the classical theory of piezoelectricity. By the way, the strain ε is defined as

$$\varepsilon_{ij} = \frac{1}{2}\left(u_{i,j} + u_{j,i}\right) \tag{10}$$

According to the reformulated strain gradient theory [32], the higher order stress can be divided into two parts:

$$\sigma^1_{ijm} = f_{ijmk}P_k \tag{11}$$

$$\sigma^2_{ijm} = g_{ijmknl}u_{k,nl} = p_i + \tau^{(1)}_{ijm} + m'_{ij} \tag{12}$$

And p_i, $\tau^{(1)}_{ijm}$ and m'_{ij} are respectively defined as

$$p_i = \frac{\partial U}{\partial \varepsilon_{nn,i}} = 2\mu l_0^2 \varepsilon_{nn,i} \tag{13}$$

$$\tau^{(1)}_{ijk} = \frac{\partial U}{\partial \eta^{(1)}_{ijk}} = 2\mu l_1^2 \eta^{(1)}_{ijk} \tag{14}$$

$$m'_{ij} = \frac{\partial U}{\partial \chi'_{ij}} = 2\mu\left(l_2^2 + \frac{9}{5}l_0^2\right)\chi'_{ij} + 2\mu\left(l_2^2 - \frac{9}{5}l_0^2\right)\chi'_{ji} \tag{15}$$

where μ is the shear modulus, l_0, l_1, and l_2 are the additional independent material length scale parameters associated with the dilatation gradients, deviatoric stretch gradients, and symmetric rotation gradients, respectively.

While the deviatoric stretch gradient tensor $\eta^{(1)}_{ijk}$ and the symmetric rotation tensor χ'_{ij} are defined by

$$\begin{aligned}\eta^{(1)}_{ijk} &= \eta^s_{ijk} - \eta^{(0)}_{ijk} \\ &= \frac{1}{3}\left(\varepsilon_{ij,k} + \varepsilon_{jk,i} + \varepsilon_{ki,j}\right) - \frac{1}{15}\left(\delta_{ij}(2\varepsilon_{mk,m} + \varepsilon_{mm,k}) + \delta_{jk}(2\varepsilon_{mi,m} + \varepsilon_{mm,i})\right. \\ &\quad \left. + \delta_{ki}\left(2\varepsilon_{mj,m} + \varepsilon_{mm,j}\right)\right)\end{aligned} \tag{16}$$

$$\chi'_{ij} = e_{ipq}\eta'_{pqj} = e_{ipq}\varepsilon'_{jq,p} = e_{ipq}\left(\varepsilon_{jq,p} - \frac{1}{3}\delta_{qj}\varepsilon_{nn,p}\right) \tag{17}$$

where δ_{ij} and e_{ijk} are the Kronecker symbol and the alternating symbol, respectively.

3. Formulation of a dielectric nanobeam

In this paper, attention is focused on the bending behavior of a piezoelectric nanobeam of length L, thickness h, and width b with external transverse force (F) applied at the central or end points and different boundary conditions, as shown in Fig. 1. A Cartesian coordinate system is used to describe the beam with the x-axis being the centroidal axis of the undeformed beam, and the z-axis being along the thickness direction. A constant electric potential V is applied between the upper surface ($z = h/2$) and the lower surface ($z = -h/2$) of the beam and the beam is polarized along the z axis. Assuming the transverse displacement of the bending beam is denoted as $w(x)$, the displacement at any point of the piezoelectric beam can be expressed under the Euler beam hypotheses as

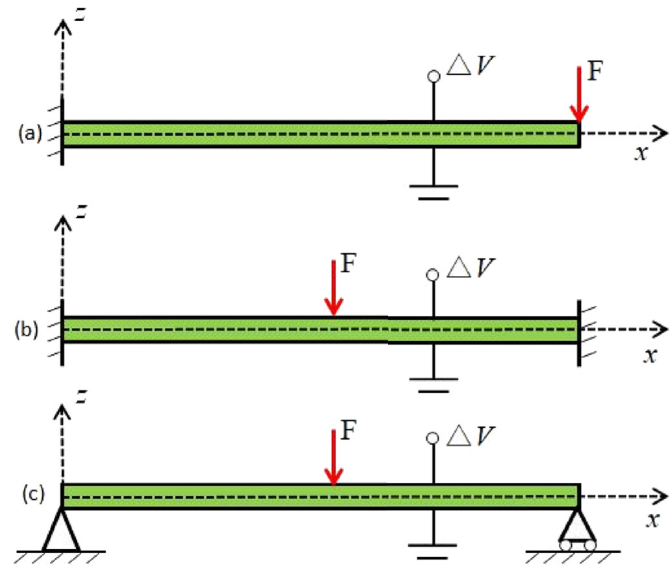

Fig. 1. Schematic of piezoelectric nanobeams with various boundary conditions (a) Cantilever beam, (b) Clamped-Clamped beam, and (c) Simply supported beam.

$$\begin{aligned}u_1(x,z) &= u_0(x) - z\frac{dw(x)}{dx} \\ u_2(x,z) &= 0 \\ u_3(x,z) &= w(x)\end{aligned} \tag{18}$$

Where $u_0(x)$ is the axial displacement along the centroidal axis of the beam, which may be induced by the applied mechanical load, the applied electrical load due to the electromechanical coupling, or the flexoelectric effect.

By substituting Eq. (18) into Eq. (10), then the non-zero strain ε_{ij} is

$$\varepsilon_{11} = \frac{\partial u_0}{\partial x} - z\frac{\partial^2 w}{\partial x^2} \tag{19}$$

and the dilatation gradient vector $\varepsilon_{ij,k}$ is

$$\begin{aligned}\varepsilon_{11,1} &= \frac{\partial^2 u_0}{\partial x^2} - z\frac{\partial^3 w}{\partial x^3} \\ \varepsilon_{11,3} &= -\frac{\partial^2 w}{\partial x^2}\end{aligned} \tag{20}$$

Here, $\varepsilon_{11,1}$ can be ignored as it is sufficiently small compared with $\varepsilon_{11,3}$ [19]. Then by substituting Eq. (19) and Eq. (20) into Eq. (16) and Eq. (17), the non-zero components of the deviatoric stretch gradient tensor $\eta^{(1)}_{ijk}$ and the symmetric rotation tensor χ'_{ij} are

$$\begin{aligned}\eta^{(1)}_{333} &= \frac{1}{5}\frac{\partial^2 w}{\partial x^2} \\ \eta^{(1)}_{113} = \eta^{(1)}_{131} = \eta^{(1)}_{311} &= -\frac{4}{15}\frac{\partial^2 w}{\partial x^2} \\ \eta^{(1)}_{223} = \eta^{(1)}_{232} = \eta^{(1)}_{322} &= \frac{1}{15}\frac{\partial^2 w}{\partial x^2}\end{aligned} \tag{21}$$

$$\begin{aligned}\chi'_{12} &= -\frac{1}{3}\frac{\partial^2 w}{\partial x^2} \\ \chi'_{21} &= -\frac{2}{3}\frac{\partial^2 w}{\partial x^2}\end{aligned} \tag{22}$$

The electric field is assumed to exist only in the beam thickness direction [37], in which the electric field component in the length direction was negligible compared with that in the thickness direction for a piezoelectric nanobeam under an electric potential across its thickness. That means $E_1 = E_2 = 0$. In the formulation of what followed, the matrix notations are introduced for convenience, i.e., $c_{11} = c_{1111}$ and $d_{31} = d_{311}$. From Eqs. (9), (18)–(20), the electric field in z-direction can be written as

$$E_3 = a_{33}P_3 + d_{31}\left(\frac{\partial u_0}{\partial x} - z\frac{\partial^2 w}{\partial x^2}\right) - f_{13}\frac{d^2 w}{dx^2} \tag{23}$$

in which the extra term $-f_{13}d^2w/dx^2$ is different from the linear piezoelectricity theory and attributes to the flexoelectric effect.

In the absence of free body charges, Gauss's law is reformulated as

$$-e_0\frac{\partial^2 \Phi}{\partial z^2} + \frac{\partial P_3}{\partial z} = 0 \tag{24}$$

where Φ is the electric potential and is related to the electric field by

$$E_3 = -\frac{\partial \Phi}{\partial z} \tag{25}$$

with the consideration of the electric boundary conditions

$$\Phi(h/2) = \Delta V \ \ and \ \ \Phi(-h/2) = 0 \tag{26}$$

The polarization and the electric field can be determined in terms of u_0 and w from Eqs. (23)–(26) as

$$\begin{aligned} P_3 &= \frac{e_0 d_{31}}{e_0 a_{33}+1} z\frac{\partial^2 w}{\partial x^2} - \frac{d_{31}}{a_{33}}\frac{\partial u_0}{\partial x} + \frac{f_{13}}{a_{33}}\frac{d^2 w}{dx^2} - \frac{\Delta V}{a_{33}h} \\ E_3 &= -\frac{z d_{31}}{e_0 a_{33}+1}\frac{\partial^2 w}{\partial x^2} - \frac{\Delta V}{h} \end{aligned} \tag{27}$$

By substituting Eqs. (19) and (27) into Eq. (7), the axial stress σ_{11} can be written as

$$\sigma_{11} = \left(c_{11} - \frac{d_{31}^2}{a_{33}}\right)\frac{\partial u_0}{\partial x} - \left(c_{11} - \frac{e_0 d_{31}^2}{e_0 a_{33}+1}\right) z\frac{\partial^2 w}{\partial x^2} + \frac{d_{31}f_{13}}{a_{33}}\frac{\partial^2 w}{\partial x^2} - \frac{d_{31}}{a_{33}}\frac{\Delta V}{h} \tag{28}$$

Then an axial force can be written as

$$T_1 = b\int_{-\frac{h}{2}}^{\frac{h}{2}} \sigma_{11} dz = bh\left[\left(c_{11} - \frac{d_{31}^2}{a_{33}}\right)\frac{\partial u_0}{\partial x} + \frac{d_{31}f_{13}}{a_{33}}\frac{\partial^2 w}{\partial x^2} - \frac{d_{31}}{a_{33}}\frac{\Delta V}{h}\right] \tag{29}$$

which originates from the strain, the electromechanical couplings induced by the strain gradient, and the applied electrical load. For a Clamped-Clamped (C-C) or Simply supported-Simply supported (S-S) beam, the axial displacement is restricted to be zero ($u_0 = 0$). Thus the resultant force becomes

$$T_1 = bh\left(\frac{d_{31}f_{13}}{a_{33}}\frac{\partial^2 w}{\partial x^2} - \frac{d_{31}}{a_{33}}\frac{\Delta V}{h}\right) \tag{30}$$

which is expected to influence the bending behavior of the C-C and S-S beams. It is noted that mechanical buckling may occur when the axial force is compressive and increases beyond a critical value. This point is out of the scope of this work. While for the cantilever (C-F) beam, the axial force is ignored due to the free end constraint.

By substituting Eq. (27) into Eq. (11), the higher order stress σ_{ijm}^1 induced by flexoelectricity can be written as

$$\sigma_{113}^1 = f_{13}\left[\left(\frac{e_0 d_{31}}{e_0 a_{33}+1} z + \frac{f_{13}}{a_{33}}\right)\frac{\partial^2 w}{\partial x^2} - \frac{d_{31}}{a_{33}}\frac{\partial u_0}{\partial x} - \frac{\Delta V}{a_{33}h}\right] \tag{31}$$

By substituting Eqs. (20)–(22) into Eqs. (13)–(15), p_i, τ_{ijk}^1 and $m_{ij}^{'}$ can be written as

$$p_3 = -2\mu l_0^2\frac{\partial^2 w}{\partial x^2} \tag{32}$$

$$\begin{aligned} \tau_{333}^{(1)} &= \frac{2}{5}\mu l_1^2\frac{\partial^2 w}{\partial x^2} \\ \tau_{113}^{(1)} &= \tau_{131}^{(1)} = \tau_{311}^{(1)} = -\frac{8}{15}\mu l_1^2\frac{\partial^2 w}{\partial x^2} \\ \tau_{223}^{(1)} &= \tau_{232}^{(1)} = \tau_{322}^{(1)} = \frac{2}{15}\mu l_1^2\frac{\partial^2 w}{\partial x^2} \end{aligned} \tag{33}$$

$$\begin{aligned} m_{12}' &= \mu\left(-2l_2^2 + \frac{6}{5}l_0^2\right)\frac{\partial^2 w}{\partial x^2} \\ m_{21}' &= -\mu\left(2l_2^2 + \frac{6}{5}l_0^2\right)\frac{\partial^2 w}{\partial x^2} \end{aligned} \tag{34}$$

The energy method is used to obtain the governing equations of the bending piezoelectric nanobeam with the consideration of the flexoelectricity. From Eqs. (6)–(9), the internal energy density function is given as

$$U = \frac{1}{2}\left(\sigma_{ij}\varepsilon_{ij} + \sigma_{ijm}u_{ij,m} + E_iP_i\right) = \frac{1}{2}\left(\sigma_{11}\varepsilon_{11} + \sigma_{113}\varepsilon_{11,3} + E_3P_3\right) \tag{35}$$

On the other hand, the variation of the work done by the external distributed force $\tilde{q}(x)$, the boundary shear force F, and the boundary-bending moments M, respectively, reads

$$\delta\tilde{W} = \int_0^l \tilde{q}(x)\delta w(x)dx + \left[\overline{F}\delta w\right]\big|_0^l + \left[\overline{M}\delta w'\right]\big|_0^l \tag{36}$$

Moreover, the virtual work done by the resultant axial force for the C-C and S-S beams are defined as

$$\delta\overline{W} = -\frac{1}{2}\delta\int_0^L T_1\left(\frac{\partial w}{\partial x}\right)^2 dx \tag{37}$$

By neglecting the kinetic energy and substituting Eqs. (35)–(37) into Eq. (5), the governing equations and boundary conditions of the bending piezoelectric beams will be given as (please refer Appendix for detail).

3.1. Cantilever beam

The governing equations:

$$\begin{cases} \dfrac{d_{31}f_{13}}{a_{33}}A\dfrac{\partial^3 u_0}{\partial x^3} + \left[\left(c_{11} - \dfrac{e_0 d_{31}^2}{e_0 a_{33}+1}\right)I + \varGamma A - \dfrac{f_{13}^2}{a_{33}}A\right]\dfrac{\partial^4 w}{\partial x^4} = \tilde{q}(x) \\ \left(c_{11} - \dfrac{d_{31}^2}{a_{33}}\right)A\dfrac{\partial^2 u_0}{\partial x^2} + \dfrac{d_{31}f_{13}}{a_{33}}A\dfrac{\partial^3 w}{\partial x^3} = 0 \end{cases} \tag{38}$$

and the boundary conditions:

$$\frac{d_{31}f_{13}}{a_{33}}A\frac{\partial^2 u_0}{\partial x^2}+\left[\left(c_{11}-\frac{e_0d_{31}^2}{e_0a_{33}+1}\right)I+\Gamma A-\frac{f_{13}^2}{a_{33}}A\right]\frac{\partial^3 w}{\partial x^3}-\overline{F}=0$$

$$\text{or } \delta w=0 \; for \; x=0,\ L$$

$$\frac{d_{31}f_{13}}{a_{33}}A\frac{\partial u_0}{\partial x}+\left[\left(c_{11}-\frac{e_0d_{31}^2}{e_0a_{33}+1}\right)I+\Gamma A-\frac{f_{13}^2}{a_{33}}A\right]$$

$$\frac{\partial^2 w}{\partial x^2}+\frac{\Delta V f_{13}}{a_{33}h}A-\overline{M}=0 \tag{39}$$

$$\text{or } \delta\frac{\partial w}{\partial x}=0 \quad for \quad x=0,\ L$$

$$\left[\left(c_{11}-\frac{d_{31}^2}{a_{33}}\right)\frac{\partial^2 u_0}{\partial x^2}+\frac{d_{31}f_{13}}{a_{33}}\frac{\partial^3 w}{\partial x^3}-\frac{\Delta V d_{31}}{a_{33}h}\right]A=0$$

$$\text{or } \delta\frac{\partial u_0}{\partial x}=0 \; for \; x=0,\ L$$

$$\begin{cases} w=0 & for\ x=0\\ \frac{\partial w}{\partial x}=0 & for\ x=0\\ \left[\left(c_{11}-\frac{e_0d_{31}^2}{e_0a_{33}+1}\right)I+\Gamma A-\frac{f_{13}^2}{a_{33}}A-\frac{f_{13}^2d_{31}^2}{a_{33}\left(a_{33}c_{11}-d_{31}^2\right)}A\right]\frac{\partial^3 w}{\partial x^3}=F & for\ x=L\\ \left[\left(c_{11}-\frac{e_0d_{31}^2}{e_0a_{33}+1}\right)I+\Gamma A-\frac{f_{13}^2}{a_{33}}A-\frac{f_{13}^2d_{31}^2}{a_{33}\left(a_{33}c_{11}-d_{31}^2\right)}A\right]\frac{\partial^2 w}{\partial x^2}+\frac{c_{11}f_{13}\Delta V b}{a_{33}c_{11}-d_{31}^2}=0 & for\ x=L \end{cases} \tag{44}$$

where $\Gamma=\left(\frac{12}{5}\mu l_0^2+\frac{8}{15}\mu l_1^2+2\mu l_2^2\right)$

3.2. C-C and S-S beams

The governing equation

$$\left[\left(c_{11}-\frac{e_0d_{31}^2}{e_0a_{33}+1}\right)I+\Gamma A-\frac{f_{13}^2}{a_{33}}A\right]\frac{\partial^4 w}{\partial x^4}+b\frac{d_{31}}{a_{33}}\Delta V\frac{\partial^2 w}{\partial x^2}=\tilde{q}(x) \tag{40}$$

and the boundary conditions

$$\left[\left(c_{11}-\frac{e_0d_{31}^2}{e_0a_{33}+1}\right)I+\Gamma A-\frac{f_{13}^2}{a_{33}}A\right]\frac{\partial^3 w}{\partial x^3}+b\frac{d_{31}}{a_{33}}\Delta V\frac{\partial w}{\partial x}\delta w-\overline{F}=0$$

$$\text{or } \delta w=0 \ \ for \ \ x=0,L$$

$$\left[\left(c_{11}-\frac{e_0d_{31}^2}{e_0a_{33}+1}\right)I+\Gamma A-\frac{f_{13}^2}{a_{33}}A\right]\frac{\partial^2 w}{\partial x^2}+\frac{\Delta V f_{13}}{a_{33}h}A \tag{41}$$

$$+\frac{1}{2}bh\frac{d_{31}f_{13}}{a_{33}}\left(\frac{\partial w}{\partial x}\right)^2-\overline{M}=0$$

$$\text{or } \delta\frac{\partial w}{\partial x}=0 \; for \; x=0,L$$

Obviously, ΓA is included in the effective bending rigidity for both beam models, which originates from the strain gradient elasticity effect, while Af_{13}^2/a_{33} originates from the flexoelectricity. In another word, both strain gradient and flexoelectricity affect the bending rigidity, which will be discussed later.

3.3. Solution of boundary value problems in static bending

This sub-section deals with the solution of a boundary value problem for static bending. Assuming the three different beams subjected to a concentrated force F, as shown in Fig. 1.

For C-F beam, the concentrated force F at the end of beam, on the other hand, haven't any applied mechanical loads in the axial direction, so the force $T_1=0$. By substituting T_1 into Eq. (29), the relaxation strain can be obtained as

$$\frac{\partial u_0}{\partial x}=-\frac{d_{31}}{a_{33}c_{11}-d_{31}^2}\left(f_{13}\frac{\partial^2 w}{\partial x^2}-\frac{\Delta V}{h}\right) \tag{42}$$

The transverse displacement and slope at the end $x=0$ are zeros, $w=dw/dx=0$. The boundary condition at $x=L$ can be obtained from Eq. (39). By substituting Eq. (42)into Eqs. (38) and (39), the C-F beam's governing equation and boundary conditions will be given as

$$\left[\left(c_{11}-\frac{e_0d_{31}^2}{e_0a_{33}+1}\right)I+\Gamma A-\frac{f_{13}^2}{a_{33}}A-\frac{f_{13}^2d_{31}^2}{a_{33}\left(a_{33}c_{11}-d_{31}^2\right)}A\right]\frac{\partial^4 w}{\partial x^4}=0 \tag{43}$$

Solving governing equation (43) with consideration of the beam boundary conditions as stated Eq. (44), the explicit expressions of the transverse deflections for the C-F beam is derived as

$$w=\frac{a_{33}\left(a_{33}c_{11}-d_{31}^2\right)F(x-3L)-3a_{33}c_{11}f_{13}\Delta V b}{6\left[\Gamma A-\frac{f_{13}^2}{a_{33}}A-\frac{f_{13}^2d_{31}^2}{a_{33}\left(a_{33}c_{11}-d_{31}^2\right)}A\right]a_{33}\left(a_{33}c_{11}-d_{31}^2\right)-f_{13}^2d_{31}^2bh}x^2 \tag{45}$$

For S-S and C-C beam, the applied load $\tilde{q}(x)$ can be expanded in a Fourier series as

$$\tilde{q}(x)=\sum_{n=1}^{\infty}Q_n\sin\left(\frac{n\pi x}{L}\right) \tag{46}$$

For a given $\tilde{q}(x)$, Q_n in Eq. (46) can be readily determined to be

$$Q_n=\frac{2}{L}\int_0^L\tilde{q}(x)\sin\left(\frac{n\pi x}{L}\right)dx \tag{47}$$

In the present investigation as shown in Fig. 1, $\tilde{q}(x)=F\delta(x-L/2)$, where $\delta(\cdot)$ is the Dirac delta function and F is the concentrated force. Substituting $\tilde{q}(x)$ of Eq. (47) into Eq. (46), then it gives

$$Q_n=\frac{2}{L}F\sin\left(\frac{n\pi}{2}\right) \tag{48}$$

For an S-S beam, the boundary condition can be written as

$$\begin{cases} w=0 & for\ x=0\ and\ x=L\\ EI\frac{\partial^2 w}{\partial x^2}+\frac{\Delta V f_{13}b}{a_{33}}+\frac{f_{13}d_{31}A}{2a_{33}}\left(\frac{\partial w}{\partial x}\right)^2=0 & for\ x=0\ and\ x=L \end{cases} \tag{49}$$

in which $EI=\left(c_{11}-\frac{e_0d_{31}^2}{e_0a_{33}+1}\right)I+\Gamma A-\frac{f_{13}^2}{a_{33}}A$ and the term $\frac{f_{13}d_{31}A}{2a_{33}}\left(\frac{\partial w}{\partial x}\right)^2$ can be neglected under the infinitesimal deformation assumption. By substituting Eq. (46) into Eq. (40) and combining with Eq. (49), the transverse deflections for the S-S beam is derived as

$$w = \begin{cases} \dfrac{\Delta V f_{13} b}{a_{33} EI s_0^2}\left[1 + \dfrac{\cosh(s_0 L - 1)}{\sinh(s_0 L)}\sinh(s_0 x) - \cosh(s_0 x)\right] + \sum_{n=1}^{\infty} B_n \sin\dfrac{n\pi x}{L} & for \Delta V < 0 \\ -\dfrac{\Delta V f_{13} b}{a_{33} EI s_1^2}\left[1 + \dfrac{\cos(s_1 L - 1)}{\sin(s_1 L)}\sin(s_1 x) - \cos(s_1 x)\right] + \sum_{n=1}^{\infty} B_n \sin\dfrac{n\pi x}{L} & for \Delta V > 0 \\ \sum_{n=1}^{\infty} B_n \sin\dfrac{n\pi x}{L} & for \Delta V = 0 \end{cases} \tag{50}$$

where

$$B_n = \frac{Q_n}{EIa_n^4 - k_5 a_n^2}, \quad k_5 = \frac{\Delta V d_{31} b}{a_{33}}, a_n = n\pi/L, \quad s_0 = \sqrt{-\frac{k_5}{EI}}, \quad s_1 = \sqrt{\frac{k_5}{EI}}$$

For a C-C beam, the boundary condition is the same as that for a C-F beam at $x = 0$, the boundary condition at $x = L$ is the same as that the boundary condition at $x = 0$. So the boundary condition for a C-C beam can be written as

$$\begin{cases} w = 0 \quad \text{for } x = 0 \text{ or } x = L \\ \dfrac{\partial w}{\partial x} = 0 \quad \text{for } x = 0 \text{ or } \ x = L \end{cases} \tag{51}$$

By substituting Eq. (46) into Eq. (40) and combing with Eq. (51), the transverse deflections for the C-C beam is derived as

$$w = \begin{cases} C_1 + C_2 x + C_3 \cosh(s_0 x) + C_4 \sinh(s_0 x) + \sum_{n=1}^{\infty} B_n \sin\left(\dfrac{n\pi x}{L}\right) & \Delta V < 0 \\ D_1 + D_2 x + D_3 \cos(s_1 x) + D_4 \sin(s_1 x) + \sum_{n=1}^{\infty} B_n \sin\left(\dfrac{n\pi x}{L}\right) & \Delta V > 0 \\ -x\sum_{n=1}^{\infty} B_n a_n + \dfrac{2\sum_{n=1}^{\infty} B_n a_n + \sum_{n=1}^{\infty} B_n a_n cos(n\pi)}{L} x^2 - \dfrac{\sum_{n=1}^{\infty} B_n a_n + \sum_{n=1}^{\infty} B_n a_n cos(n\pi)}{L^2} x^3 & \Delta V = 0 \end{cases} \tag{52}$$

where C_i and D_i are given in Appendix.

4. Numerical results

In this section, the electroelastic responses of a piezoelectric nanobeam loaded with a concentrated force $F = 1$ nN and an electric potential ΔV under different boundary constraints are investigated to study the flexoelectric effect. The geometry of the beam is set as $L = 20h$ and $b = h$. The material is taken as B_aTiO_3. For a narrow beam, the material parameters are calculated as $c_{11} = 131\text{GP}_a$, $d_{31} = 1.87 \times 10^8$ V/m, and $a_{33} = 0.79 \times 10^8$ V·m/C. While the three internal material length scale parameters are taken as the same, i.e. $l_0 = l_1 = l_2 = 10$ nm. Here the beam thickness is taken as $h = 2l_0$ and the applied electrical load is $\Delta V =$ -0.1 V. The Poisson's ratio $\nu = 0.38$, Young's module is $E = 1.44\text{GP}_a$ and $f_{13} = 5$ V is adopted in the simulation. Use these parameters, all others physical quantities can be subsequently determined without any difficulty.

For simplification, for different boundary conditions (CF, CC, SS), we show the results of three models: (i) the model with both strain gradient elasticity and flexoelectricity included is called the SF model, which is the current model developed in this paper; (ii) the model with only flexoelectricity included is called the FL model and (iii) the model without both strain gradient elasticity and flexoelectricity included is called the NF model.

Firstly, the transverse displacements of C-F, S-S and C-C beams for different models (SF and FL) are plotted in Fig. 2. It is observed from Fig. 2 that the displacement of SF model is less than that of FL model, which means the strain gradient terms can decrease the displacement. It is due to the strain gradient term ΓA in the effective bending rigidity EI shown in Eqs. (38) and (40). The discrepancy of maximum displacement between the two models is almost 8%. The effect of strain gradient elasticity is also discussed in Deng's recent work [5], where the strain gradient has great effect on the normalized effective piezoelectricity and concluded that the strain gradient is significant when the sample size is small enough especially in nanoscale. The similar conclusion of the effect of the strain gradient elasticity is also observed in the work [29].

Secondly, in Fig. 3, the flexoelectric effect on the beam bending behavior can also be shown by the normalized contact stiffness k/k_0, where k is defined as the ratio of the applied force to the induced displacement where force applied and k_0 is the contact stiffness for an NF model [37]. It is shown that the normalized contact stiffness k/k_0 increases with the scaling up of the beam thickness for the beams with different boundary conditions and different models.

Moreover, no matter what kind of boundary conditions, the value of k/k_0 of the two models (SF and FL) will become closer and closer with the beam thickness increasing, which is attributed to the diminishing of the strain gradient effect for large-scale structures. Alternatively, the differences between the two models are reduced with the size scale increasing. With a smaller size scale (i.e., smaller beam dimension for the same material), the present model (SF) shows strong size effect especially in nanoscale, which, again, confirms the significant effect of strain gradient elasticity. For a C-C beam, k/k_0 approaches one due to the diminishing of the effect, while k/k_0 approaches to 1.9 and 0.34 under bias electric loading -0.1 V for the C-F and S-S beams. Such difference is the result of the non-homogeneous boundary conditions for C-F and S-S beams as shown in Eqs. (39) and (41), where ΔV is embedded. It means that the non-homogeneous condition is not only associated with the flexoelectricity, but also with the applied electrical load. Furthermore, there are no non-homogeneous boundary conditions for the C-F and S-S beams if the electrical potential equals zero, which results in the normalized contact stiffness approaching to one for all three kinds of beams with sufficiently large thickness.

Thirdly, for a C-F beam, there is no axial force along the beam, which means that Eq. (29) is equal to zero. Then, the relaxation strain is expressed as

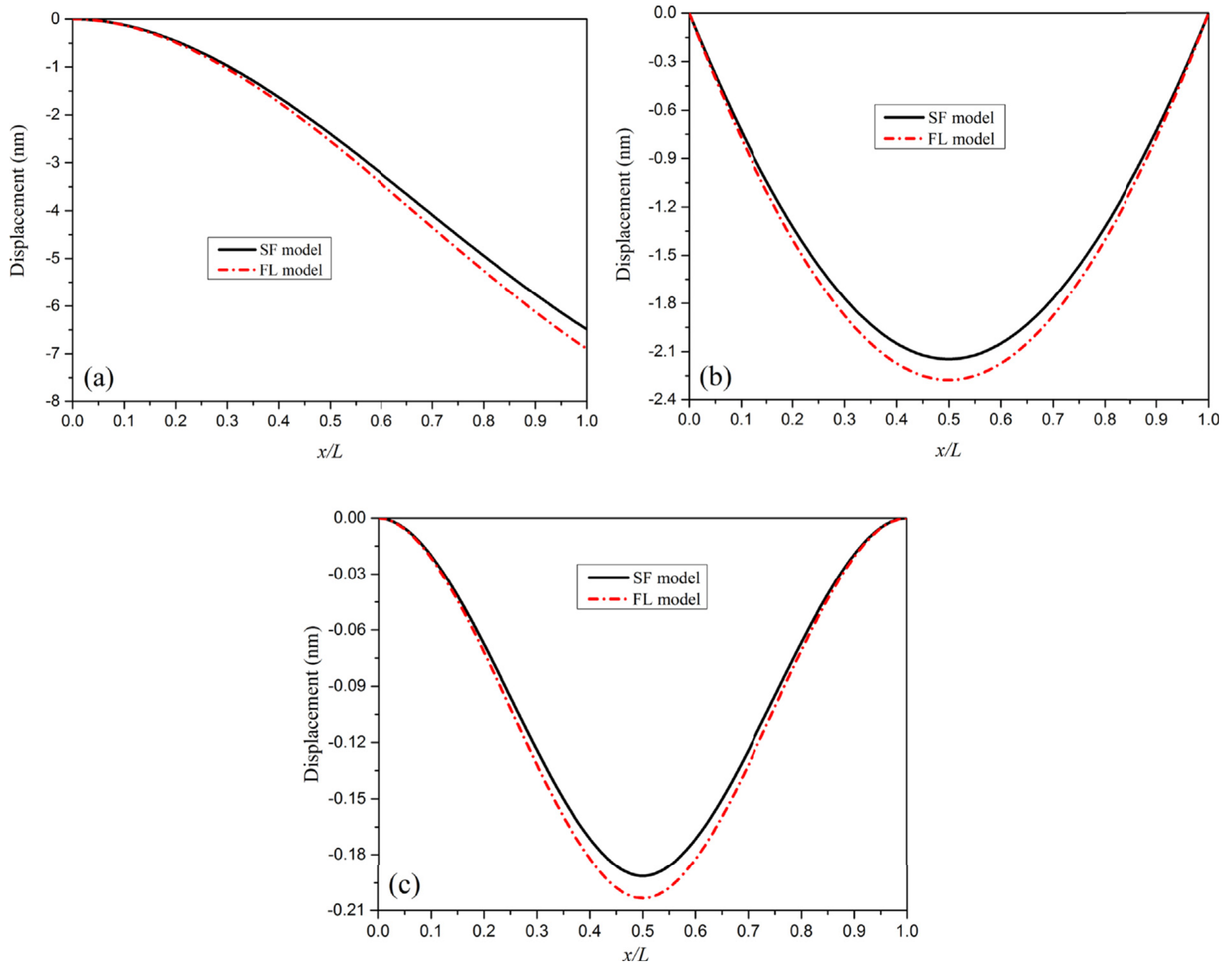

Fig. 2. Transverse displacement of C-F, S-S and C-C beams for different models.

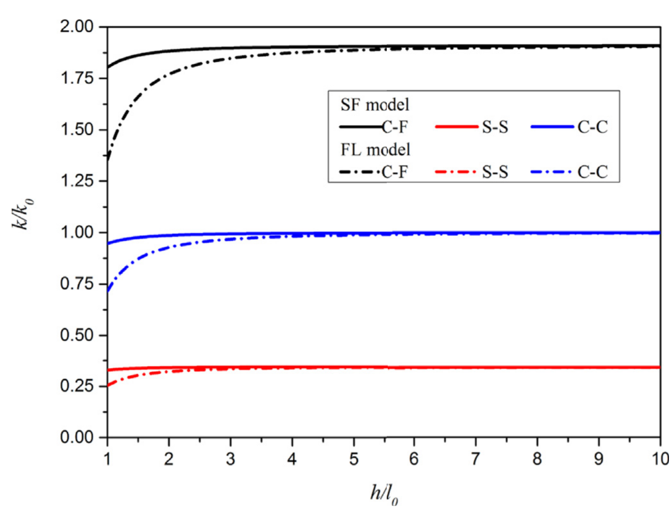

Fig. 3. Variation of normalized contact stiffness with beam thickness for beams with different boundary conditions ($\Delta V = -0.1$ V).

$$\varepsilon_0 = -\frac{d_{31}}{a_{33}c_{11} - d_{31}^2}\left(f_{13}\frac{\partial^2 w}{\partial x^2} - \frac{\Delta V}{h}\right) \tag{53}$$

It is obvious that the relaxation strain depends on not only the applied electric force but also on the longitudinal position x with flexoelectricity included. However, the relaxation strain will be independent of the longitudinal position x without considering the flexoelectricity, which results in constant relaxation strain along longitudinal position under the applied electrical loads. Therefore, to study the axial relaxation strain effect, the variation of this axial relaxation strain with beam thickness h at both ends of the beam for three models under different electrical loads are plotted in Fig. 4. Since the NF model is absent of the flexoelectricity, the relaxation strain keeps constant along the beam and there is no difference at $x = 0$ and L as shown in Fig. 4.

It is observed from Fig. 4 that the difference of relaxation strain from the SF and FL models is getting smaller with beam thickness increasing and the difference almost diminishes when h/l_0 greater than 7, which indicates that the strain gradient elasticity effect can be ignored for large h/l_0. Whereas the strain gradient cannot be ignored for the beam with its thickness is comparable to the internal material length scale parameters. It is also found in Fig. 4 that the five curves approach the same value for large beam scale, which indicates that both strain gradient elasticity and flexoelectricity effects diminish for large-scale structures. The most interesting phenomenon in Fig. 4 is that, for FL and SF models, the relaxation strain at $x = 0$ increases firstly and then decreases with h when negative voltage applied, while for other cases only monotonous values are observed. In fact, whether the relaxation strain is positive or negative depends on the values in parentheses in Eq. (53).

Fourthly, for the S-S beam and C-C beam, the axial displacement is restricted, which results in the axial force (T_1) along the beam as shown in Eq. (30). Similar to the normalized contact stiffness, Fig. 5 plots the normalized axial force T_1/T_1^0 versus the beam thickness h at $x = 0$ and L/2 for both the C-C and S-S beams in order to observe the flexoelectric effect, where T_1^0, independent of boundary conditions, is the axial force from NF model.

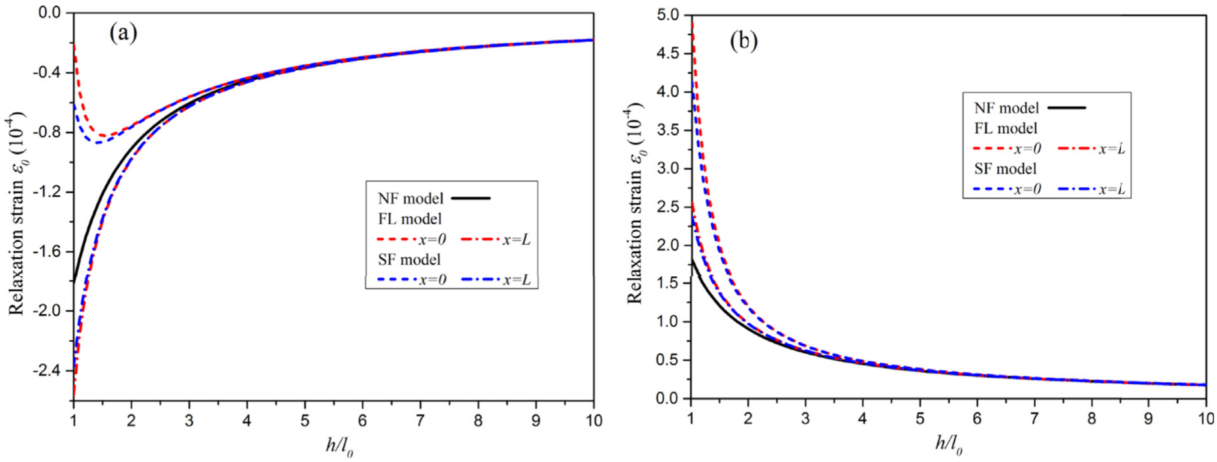

Fig. 4. Variation of relaxation strain with beam thickness for C-F beam with different electrical loads (a) $\Delta V = -0.1$ V and (b) $\Delta V = 0.1$ V.

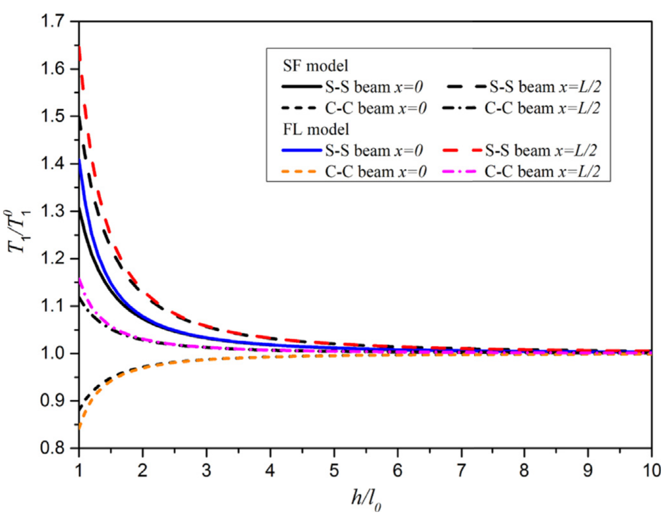

Fig. 5. Variation of normalized axial force with beam thickness for both C-C and S-S beams ($\triangle V = -0.1$ V).

It is observed from Fig. 5 that the absolute values of normalized axial force from SF model are less than those from FL model due to the inclusion of strain gradient elasticity, which is consistent with what shows in Fig. 2. It is also found that the normalized axial force for S-S beam is greater than that for the C-C beam at $x = 0$ or $L/2$. This may arise from the fact that the S-S beam undergoes greater displacement (proven in Fig. 2) and bears greater axial force consequently for the same mechanical and/or electric loading. And, as expected, all the curves approach to 1.0 with the increasing of the beam thickness h due to diminishing of the flexoelectricity and the strain gradient effects for large-scale beams.

Next, we move the focus on the electric response of the electromechanical coupling beam. The polarization of the C-F beam of different electrical loads is presented for various models as shown in Fig. 6. The electric polarization is given in Eq. (27), where the first term $\frac{e_0 d_{31} h}{2(e_0 a_{33}+1)}$ in Eq. (27) is 10^{-4}~10^{-3} times of f_{13}/a_{33} with the considered range of the beam thickness h and the material properties. Thus, the first term in P_3 can be neglected and the polarization can be regarded as uniformly distributed across the beam thickness in the bending nanobeam. And the polarization will further keep constant if flexoelectricity is ignored in Eq. (27), which is the NF model. Therefore, there is no difference along the beam at $x = 0$ and L. While the polarization are different between the FL and SF models for the same position and loading as shown in Fig. 6. However, such difference is getting smaller with beam thickness increasing. It is also noticed from Fig. (a) and (b) that the polarizations from different models approaches to the same value for the same load case, which means that the effects of strain gradient elasticity and flexoelectricity is neglectable for large h/l_0 but it is notable for nanoscale beam.

Finally, the energy efficiency Q/F for C-F beam is studied in Fig. 7, where $Q = \int P(x)dA$ is the induced charge between the bottom and upper surface of the beam with mechanical F applied only. As discussed in Fig. 6, the first term in P_3 can be neglected, which results in the much

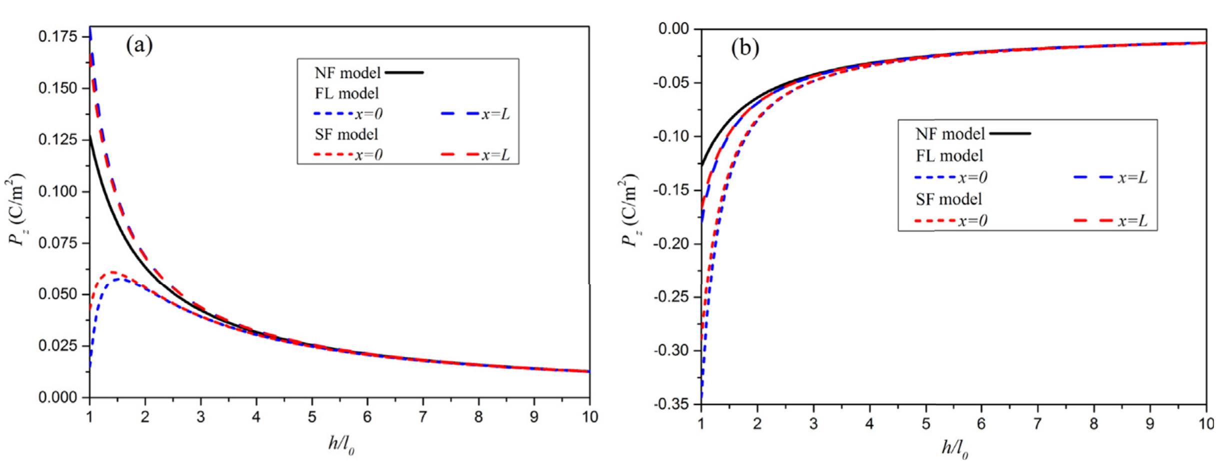

Fig. 6. Variation of polarization with beam thickness for C-F beam for different electrical loads (a) $\triangle V = -0.1$ V and (b) $\triangle V = 0.1$ V.

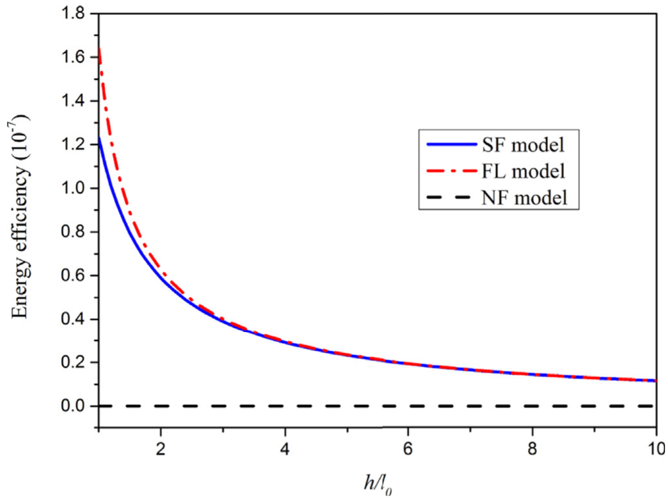

Fig. 7. Energy efficiency with beam thickness for C-F beam.

smaller energy efficiency (in the order of 10^{-11}) in Fig. 7 for the NF model compared to the SF and the FL models.

Moreover, for the SF and FL models, the energy efficiency is notable when the beam thickness is comparable to the material length scale parameter (l_0) while it decays quickly with the beam thickness increases, which means that the strain gradient effect can be neglected for large h/l_0. This phenomenon has been confirmed in the Figures discussed above. It is also found that the energy efficiency of SF model is less than that of FL model, especially for lower h/l_0. In another word, the strain gradient terms can decrease the energy efficiency slightly. The same phenomenon has also been observed in a recent work [5]. In that work, the effective piezoelectricity d^{eff} with strain gradient elasticity included is nonlinear and less than that from the simplified model without including strain gradient elasticity. The work indicated the strain gradient elasticity is important. Inspired by Qian's work [5], the strain gradient term in this paper is from a strain gradient elasticity theory with three material length scale parameters.

5. Conclusion

To accurately predict the flexoelectric response of nanobeam-based energy harvesting, a reformulated strain gradient elasticity theory is employed to derive an electromechanical model of nanobeam. The governing equations and boundary conditions are derived for the cantilever, both end-clamped and both end-simply supported beams separately. The closed-form analytical solutions are obtained for the bending response of a nanobeam subject to electromechanical loads. We find that the effect of strain gradient, as well as the effect of flexoelectricity, may decay gradually with beam thickness increasing to submicron or micron. These results agree well with those from the reduced models in the case of large-scale structures, which verify that the strain gradient can be omitted. In contrast, when the thickness of beam is comparable to the material length scale parameters, we show the critical role of the strain gradient elasticity in the electromechanical coupling. This highly nonlinear coupling would significantly impact the displacement, contact stiffness, relaxation strain, axial force, polarization, and energy efficiency of a dielectric nanobeam incorporating the flexoelectricity. We hope this paper can make a good understanding of the fundamental issue of flexoelectricity and can be helpful for the design of nanoscale flexoelectric energy harvesters.

Acknowledgements

The work is supported by the Natural Science Fund of Shandong Province of China (ZR2017MA037) and China Scholarship Council.

Appendix A. Supplementary data

Supplementary data related to this article can be found at https://doi.org/10.1016/j.physe.2017.12.037.

Appendix

The variation terms in Eq. (35) when deriving the governing equations and boundary conditions are listed as follows,

$$\begin{aligned}
&\delta\int_\Omega \sigma_{11}\varepsilon_{11}d\Omega = \delta\int_\Omega\left(\left[\left(c_{11}-\frac{d_{31}^2}{a_{33}}\right)\frac{\partial u_0}{\partial x}-\left(c_{11}-\frac{e_0d_{31}^2}{e_0a_{33}+1}\right)z\frac{\partial^2 w}{\partial x^2}+\frac{d_{31}f_{13}}{a_{33}}\frac{\partial^2 w}{\partial x^2}-\frac{d_{31}}{a_{33}}\frac{\Delta V}{h}\right]\right.\\
&\left.\left(\frac{\partial u_0}{\partial x}-z\frac{\partial^2 w}{\partial x^2}\right)d\Omega = \int_0^l\left[\frac{d_{31}f_{13}}{a_{33}}A\frac{\partial^3 u_0}{\partial x^3}+2\left(c_{11}-\frac{e_0d_{31}^2}{e_0a_{33}+1}\right)I\frac{\partial^4 w}{\partial x^4}\right]\delta w\right.\\
&-\left[2\left(c_{11}-\frac{d_{31}^2}{a_{33}}\right)\frac{\partial^2 u_0}{\partial x^2}+\frac{d_{31}f_{13}}{a_{33}}\frac{\partial^3 w}{\partial x^3}\right]A\delta u_0dx\\
&+\left[2\left(c_{11}-\frac{d_{31}^2}{a_{33}}\right)\frac{\partial u_0}{\partial x}+\frac{d_{31}f_{13}}{a_{33}}\frac{\partial^2 w}{\partial x^2}-\frac{d_{31}}{a_{33}}\frac{\Delta V}{h}\right]A\delta u_0\Big|_0^l-\left[\frac{d_{31}f_{13}}{a_{33}}A\frac{\partial^2 u_0}{\partial x^2}+2\left(c_{11}-\frac{e_0d_{31}^2}{e_0a_{33}+1}\right)I\frac{\partial^3 w}{\partial x^3}\right]\delta w\Big|_0^l+\left[\frac{d_{31}f_{13}}{a_{33}}A\frac{\partial u_0}{\partial x}+2\left(c_{11}-\frac{e_0d_{31}^2}{e_0a_{33}+1}\right)I\frac{\partial w}{\partial x}\right]\delta\frac{\partial w}{\partial x}\Big|_0^l
\end{aligned} \tag{A1}$$

$$\begin{aligned}
&\delta\int_\Omega \sigma_{113}\varepsilon_{11,3}d\Omega = \delta\int_\Omega\left(\sigma_{113}^1\varepsilon_{11,3}+p_i\varepsilon_{nn,i}+\tau_{ijm}^{(1)}\eta_{ijk}^{(1)}+m_{ij}'\chi_{ij}'\right)d\Omega\\
&=\int_0^l\left\{2\left[\left(\frac{12}{5}\mu l_0^2+\frac{8}{15}\mu l_1^2+2\mu l_2^2\right)A-\frac{f_{13}^2}{a_{33}}A\right]\frac{\partial^4 w}{\partial x^4}+\frac{d_{31}f_{13}}{a_{33}}A\frac{\partial^3 u_0}{\partial x^3}\right\}\delta w-\frac{d_{31}f_{13}}{a_{33}}A\frac{\partial^3 w}{\partial x^3}\delta u_0dx-\left\{2\left[\left(\frac{12}{5}\mu l_0^2+\frac{8}{15}\mu l_1^2+2\mu l_2^2\right)A-\frac{f_{13}^2}{a_{33}}A\right]\frac{\partial^3 w}{\partial x^3}\right.\\
&\left.+\frac{d_{31}f_{13}}{a_{33}}A\frac{\partial^2 u_0}{\partial x^2}\right\}\delta w\Big|_0^l+\frac{d_{31}f_{13}}{a_{33}}A\frac{\partial^2 w}{\partial x^2}\delta u_0\Big|_0^l+\left\{2\left[\left(\frac{12}{5}\mu l_0^2+\frac{8}{15}\mu l_1^2+2\mu l_2^2\right)A-\frac{f_{13}^2}{a_{33}}A\right]\frac{\partial^2 w}{\partial x^2}+\frac{d_{31}f_{13}}{a_{33}}A\frac{\partial u_0}{\partial x}+\frac{\Delta Vf_{13}}{a_{33}h}A\right\}\delta\frac{\partial w}{\partial x}\Big|_0^l
\end{aligned} \tag{A2}$$

$$\begin{aligned}\delta\int_{\Omega} e_0 E_3 E_3 d\Omega &= \delta\int_{\Omega} e_0\left(-\frac{d_{31}}{e_0 a_{33}+1} z\frac{\partial^2 w}{\partial x^2}-\frac{\Delta V}{h}\right)-\frac{d_{31}}{e_0 a_{33}+1} z\frac{\partial^2 w}{\partial x^2}-\frac{\Delta V}{h})d\Omega \\ &= \int_0^l \frac{2e_0 d_{31}^2}{(e_0 a_{33}+1)^2} I\frac{\partial^4 w}{\partial x^4}\delta w dx-\frac{2e_0 d_{31}^2}{(e_0 a_{33}+1)^2} I\frac{\partial^3 w}{\partial x^3}\delta w|_0^l+\frac{2e_0 d_{31}^2}{(e_0 a_{33}+1)^2} I\frac{\partial^2 w}{\partial x^2}\delta\frac{\partial w}{\partial x}|_0^l\end{aligned} \tag{A3}$$

$$\begin{aligned}\delta\int_{\Omega} E_3 P_3 d\Omega &= \delta\int_{\Omega}\left(-\frac{d_{31}}{e_0 a_{33}+1} z\frac{\partial^2 w}{\partial x^2}-\frac{\Delta V}{h}\right)\left(\frac{e_0 d_{31}}{e_0 a_{33}+1} z\frac{\partial^2 w}{\partial x^2}-\frac{d_{31}}{a_{33}}\frac{\partial u_0}{\partial x}+\frac{f_{13}}{a_{33}}\frac{\partial^2 w}{\partial x^2}-\frac{\Delta V}{a_{33}h}\right)d\Omega \\ &= \int_0^l -\frac{2e_0 d_{31}^2}{(e_0 a_{33}+1)^2} I\frac{\partial^4 w}{\partial x^4}\delta w dx+\frac{2e_0 d_{31}^2}{(e_0 a_{33}+1)^2} I\frac{\partial^3 w}{\partial x^3}\delta w|_0^l-\left(\frac{2e_0 d_{31}^2}{(e_0 a_{33}+1)^2} I\frac{\partial^2 w}{\partial x^2}+\frac{f_{13}\Delta V}{a_{33}h}A\right)\delta\frac{\partial w}{\partial x}|_0^l+\frac{d_{31}\Delta V}{a_{33}h}A\delta u_0|_0^l\end{aligned} \tag{A4}$$

The coefficients C_i and D_i in Eq. (52) are:

$$\begin{aligned}
C_1 &= -\frac{\left(\sum_{n=1}^{\infty} B_n a_n\right) s_0 L(\cosh(s_0 L)-1)+\left[\left(\sum_{n=1}^{\infty} B_n a_n\cos(n\pi)\right)-\left(\sum_{n=1}^{\infty} B_n a_n\right)\right](\sinh(s_0 L)-s_0 L)}{s_0\left[(\cosh(s_0 L)-1)^2-\sinh(s_0 L)(\sinh(s_0 L)-s_0 L)\right]} \\
C_2 &= \frac{\left(\sum_{n=1}^{\infty} B_n a_n\right)(\sinh^2(s_0 L)-\cosh^2(s_0 L))+\left[\left(\sum_{n=1}^{\infty} B_n a_n\cos(n\pi)\right)+\left(\sum_{n=1}^{\infty} B_n a_n\right)\right]\cosh(s_0 L)-1}{(\cosh(s_0 L)-1)^2-\sinh(s_0 L)(\sinh(s_0 L)-s_0 L)} \\
C_3 &= \frac{\left(\sum_{n=1}^{\infty} B_n a_n\right) s_0 L(\cosh(s_0 L)-1)+\left[\left(\sum_{n=1}^{\infty} B_n a_n\cos(n\pi)\right)-\left(\sum_{n=1}^{\infty} B_n a_n\right)\right](\sinh(s_0 L)-s_0 L)}{s_0\left[(\cosh(s_0 L)-1)^2-\sinh(s_0 L)(\sinh(s_0 L)-s_0 L)\right]} \\
C_4 &= \frac{\left[\left(\sum_{n=1}^{\infty} B_n a_n\right)-\left(\sum_{n=1}^{\infty} B_n a_n\cos(n\pi)\right)\right](\cosh(s_0 L)-1)-\left(\sum_{n=1}^{\infty} B_n a_n\right)s_0 L\sinh(s_0 L)}{s_0\left[(\cosh(s_0 L)-1)^2-\sinh(s_0 L)(\sinh(s_0 L)-s_0 L)\right]}
\end{aligned} \tag{A5}$$

$$\begin{aligned}
D_1 &= \frac{\left[\left(\sum_{n=1}^{\infty} B_n a_n\right)-\left(\sum_{n=1}^{\infty} B_n a_n\cos(n\pi)\right)\right]\sin(s_1 L)+s_1 L\left[\left(\sum_{n=1}^{\infty} B_n a_n\cos(n\pi)\right)-\left(\sum_{n=1}^{\infty} B_n a_n\right)\cos(s_1 L)\right]}{s_1\left[(\cos(s_1 L)-1)^2-\sin(s_1 L)(s_1 L-\sin(s_1 L))\right]} \\
D_2 &= \frac{\left[\left(\sum_{n=1}^{\infty} B_n a_n\cos(n\pi)\right)-\left(\sum_{n=1}^{\infty} B_n a_n\right)\cos(s_1 L)\right][\cos(s_1 L)-1]-\left(\sum_{n=1}^{\infty} B_n a_n\right)\sin^2(s_1 L)}{(\cos(s_1 L)-1)^2-\sin(s_1 L)(s_1 L-\sin(s_1 L))} \\
D_3 &= -\frac{\left[\left(\sum_{n=1}^{\infty} B_n a_n\right)-\left(\sum_{n=1}^{\infty} B_n a_n\cos(n\pi)\right)\right]\sin(s_1 L)+s_1 L\left[\left(\sum_{n=1}^{\infty} B_n a_n\cos(n\pi)\right)-\left(\sum_{n=1}^{\infty} B_n a_n\right)\cos(s_1 L)\right]}{s_1\left[(\cos(s_1 L)-1)^2-\sin(s_1 L)(s_1 L-\sin(s_1 L))\right]} \\
D_4 &= \frac{\left[\left(\sum_{n=1}^{\infty} B_n a_n\right)-\left(\sum_{n=1}^{\infty} B_n a_n\cos(n\pi)\right)\right][\sin(s_1 L)-1]+\left(\sum_{n=1}^{\infty} B_n a_n\right)s_1 L\sin(s_1 L)}{s_1\left[(\cos(s_1 L)-1)^2-\sin(s_1 L)(s_1 L-\sin(s_1 L))\right]}
\end{aligned} \tag{A6}$$

References

[1] X. Wang, J. Song, F. Zhang, C. He, Z. Hu, Z. Wang, Electricity generation based on one-dimensional group-III nitride nanomaterials, Adv. Mater. 22 (2010) 2155–2158.
[2] J.D. Madden, N.A. Vandesteeg, P.A. Anquetil, P.G. Madden, A. Takshi, R.Z. Pytel, S.R. Lafontaine, P.A. Wieringa, I.W. Hunter, Artificial muscle technology: physical principles and naval prospects, IEEE J. Ocean. Eng. 29 (2004) 706–728.
[3] M. Labanca, F. Azzola, R. Vinci, L.F. Rodella, Piezoelectric surgery: twenty years of use, Br. J. Oral Maxillofac. Surg. 46 (2008) 265–269.
[4] Q. Deng, L. Liu, P. Sharma, Flexoelectricity in soft materials and biological membranes, J. Mech. Phys. Solid. 62 (2014) 209–227.
[5] Q. Deng, Size-dependent flexoelectric response of a truncated cone and the consequent ramifications for the experimental measurement of flexoelectric properties, J. Appl. Mech. 84 (2017), 101007.
[6] R.B. Meyer, Piezoelectric effects in liquid crystals, Phys. Rev. Lett. 22 (1969) 918–921.
[7] B. Chu, D. Salem, Flexoelectricity in several thermoplastic and thermosetting polymers, Appl. Phys. Lett. 101 (2012), 103905.
[8] W. Ma, L.E. Cross, Strain-gradient-induced electric polarization in lead zirconate titanate ceramics, Appl. Phys. Lett. 82 (2003) 3293–3295.
[9] N.D. Sharma, R. Maranganti, P. Sharma, On the possibility of piezoelectric nanocomposites without using piezoelectric materials, J. Mech. Phys. Solid. 55 (2007) 2328–2350.
[10] S.P. Shen, S.L. Hu, A theory of flexoelectricity with surface effect for elastic dielectrics, J. Mech. Phys. Solid. 58 (2010) 665–677.
[11] M. Gharbi, Z.H. Sun, P. Sharma, K. White, The origins of electromechanical indentation size effect in ferroelectrics, Appl. Phys. Lett. 95 (2009), 142901.
[12] M. Gharbi, Z.H. Sun, P. Sharma, K. White, S. El-Borgi, Flexoelectric properties of ferroelectrics and the nanoindentation size-effect, Int. J. Solid Struct. 48 (2011) 249–256.
[13] M.S. Majdoub, P. Sharma, T. Cagin, Enhanced size-dependent piezoelectricity and elasticity in nanostructures due to the flexoelectric effect, Phys. Rev. B 77 (2008), 125424.
[14] J.W. Hong, D. Vanderbilt, First-principles theory and calculation of flexoelectricity, Phys. Rev. B 88 (2013), 174107.
[15] F. Deng, Q. Deng, W. Yu, S. Shen, Mixed finite elements for flexoelectric solids, J. Appl. Mech. 84 (2017) 081004–081012.
[16] Z. Shuwen, L. Xu, X. Minglong, F. Bo, S. Shengping, Shear flexoelectric response along 3121 direction in polyvinylidene fluoride, Appl. Phys. Lett. 107 (2015), 142902.
[17] S. Krichen, P. Sharma, Flexoelectricity: a perspective on an unusual electromechanical coupling, J. Appl. Mech.-Trans. ASME 83 (2016) 5.

[18] P. Mohammadi, L.P. Liu, P. Sharma, A theory of flexoelectric membranes and effective properties of heterogeneous membranes, J. Appl. Mech.-Trans. ASME 81 (2014), 011007.
[19] Q. Deng, M. Kammoun, A. Erturk, P. Sharma, Nanoscale flexoelectric energy harvesting, Int. J. Solid Struct. 51 (2014) 3218–3225.
[20] S. Yang, X. Zhao, P. Sharma, Revisiting the instability and bifurcation behavior of soft dielectrics, J. Appl. Mech. 84 (2017) 031008.
[21] S. Yang, X. Zhao, P. Sharma, Avoiding the pull-in instability of a dielectric elastomer film and the potential for increased actuation and energy harvesting, Soft Matter 13 (2017) 4552–4558.
[22] S.M. Kogan, Piezoelectric effect during inhomogeneous deformation and acoustic scattering of carriers in crystals, Sov. Phys. Solid State 5 (1964) 2069–2070.
[23] L. Liu, P. Sharma, Emergent electromechanical coupling of electrets and some exact relations — the effective properties of soft materials with embedded external charges and dipoles, J. Mech. Phys. Solid. 112 (2018) 1–24.
[24] N.A. Fleck, G.M. Muller, M.F. Ashby, J.W. Hutchinson, Strain gradient plasticity-theory and experiment, Acta Metall. Mater. 42 (1994) 475–487.
[25] J. Lei, Y. He, S. Guo, Z. Li, D. Liu, Size-dependent vibration of nickel cantilever microbeams: experiment and gradient elasticity, AIP Adv. 6 (2016), 105202.
[26] I. Vardoulakis, G. Exadaktylos, S.K. Kourkoulis, Bending of marble with intrinsic length scales: a gradient theory with surface energy and size effects, J. Phys. IV Fr. 8 (1998) 399–406.
[27] D.C.C. Lam, F. Yang, A.C.M. Chong, J. Wang, P. Tong, Experiments and theory in strain gradient elasticity, J. Mech. Phys. Solid. 51 (2003) 1477–1508.
[28] H. Sadeghian, H. Goosen, A. Bossche, B. Thijsse, F. van Keulen, On the size-dependent elasticity of silicon nanocantilevers: impact of defects, J. Phys. Appl. Phys. 44 (2011), 072001.
[29] L. Zhang, B. Wang, S. Zhou, Y. Xue, Modeling the size-dependent nanostructures: incorporating the bulk and surface effects, J. Nanomech. Micromech. 7 (2017), 04016012.
[30] R.D. Mindlin, Micro-structure in linear elasticity, Arch. Ration. Mech. Anal. 16 (1964) 51–78.
[31] R.D. Mindlin, N.N. Eshel, On first strain-gradient theories in linear elasticity, Int. J. Solid Struct. 4 (1968) 109–124.
[32] S. Zhou, A. Li, B. Wang, A reformulation of constitutive relations in the strain gradient elasticity theory for isotropic materials, Int. J. Solid Struct. 80 (2016) 28–37.
[33] A.C. Eringen, On differential-equations of nonlocal elasticity and solutions of screw dislocation and surface-waves, J. Appl. Phys. 54 (1983) 4703–4710.
[34] F. Yang, A.C.M. Chong, D.C.C. Lam, P. Tong, Couple stress based strain gradient theory for elasticity, Int. J. Solid Struct. 39 (2002) 2731–2743.
[35] M.E. Gurtin, A.I. Murdoch, A continuum theory of elastic material surfaces, Arch. Ration. Mech. Anal. 57 (1975) 291–323.
[36] N. Fleck, J. Hutchinson, A reformulation of strain gradient plasticity, J. Mech. Phys. Solid. 49 (2001) 2245–2271.
[37] Z. Yan, L.Y. Jiang, Flexoelectric effect on the electroelastic responses of bending piezoelectric nanobeams, J. Appl. Phys. 113 (2013), 194102.
[38] Z. Yan, Modeling of a nanoscale flexoelectric energy harvester with surface effects, Phys. E Low-dimens. Syst. Nanostruct. 88 (2017) 125–132.
[39] R. Zhang, X. Liang, S. Shen, A Timoshenko dielectric beam model with flexoelectric effect, Meccanica 51 (2016) 1181–1188.